Check for updates

Techniques for Stereotactic Neurosurgery: Beyond the Frame, Toward the Intraoperative Magnetic Resonance Imaging—Guided and Robot-Assisted Approaches

Ziyan Guo[1], Martin Chun-Wing Leong[1], Hao Su[2], Ka-Wai Kwok[1], Danny Tat-Ming Chan[3], Wai-Sang Poon[3]

The development of stereotaxy can be dated back 100 years. However, most stereotactic neurosurgery still relies on the workflow established about half a century ago. With the arrival of computer-assisted navigation, numerous studies to improve the neurosurgical technique have been reported, leading to frameless and magnetic resonance imaging (MRI)-guided/verified techniques. Frameless stereotaxy has been proved to be comparable to frame-based stereotaxy in accuracy, diagnostic yield, morbidity, and mortality. The incorporation of intraoperative MRI guidance in frameless techniques is considered an appealing method that could simplify workflow by reducing coregistration errors in different imaging modalities, conducting general anesthesia, and monitoring the surgical progress. In light of this situation, manually operated platforms have emerged for MRI-guided frameless procedures. However, these procedures could still be complicated and time-consuming because of the intensive manual operation required. To further simplify the procedure and enhance accuracy, robotics was introduced. Robots have superior capabilities over humans in certain tasks, especially those that are limited by space, accuracy demanding, intensive, and tedious. Clinical benefits have been shown in the recent surge of robot-assisted surgical interventions. We review the state-of-the-art intraoperative MRI-guided robotic platforms for stereotactic neurosurgery. To improve the surgical workflow and achieve greater clinical penetration, 3 key enabling techniques are proposed with emphasis on their current status, limitations, and future trends.
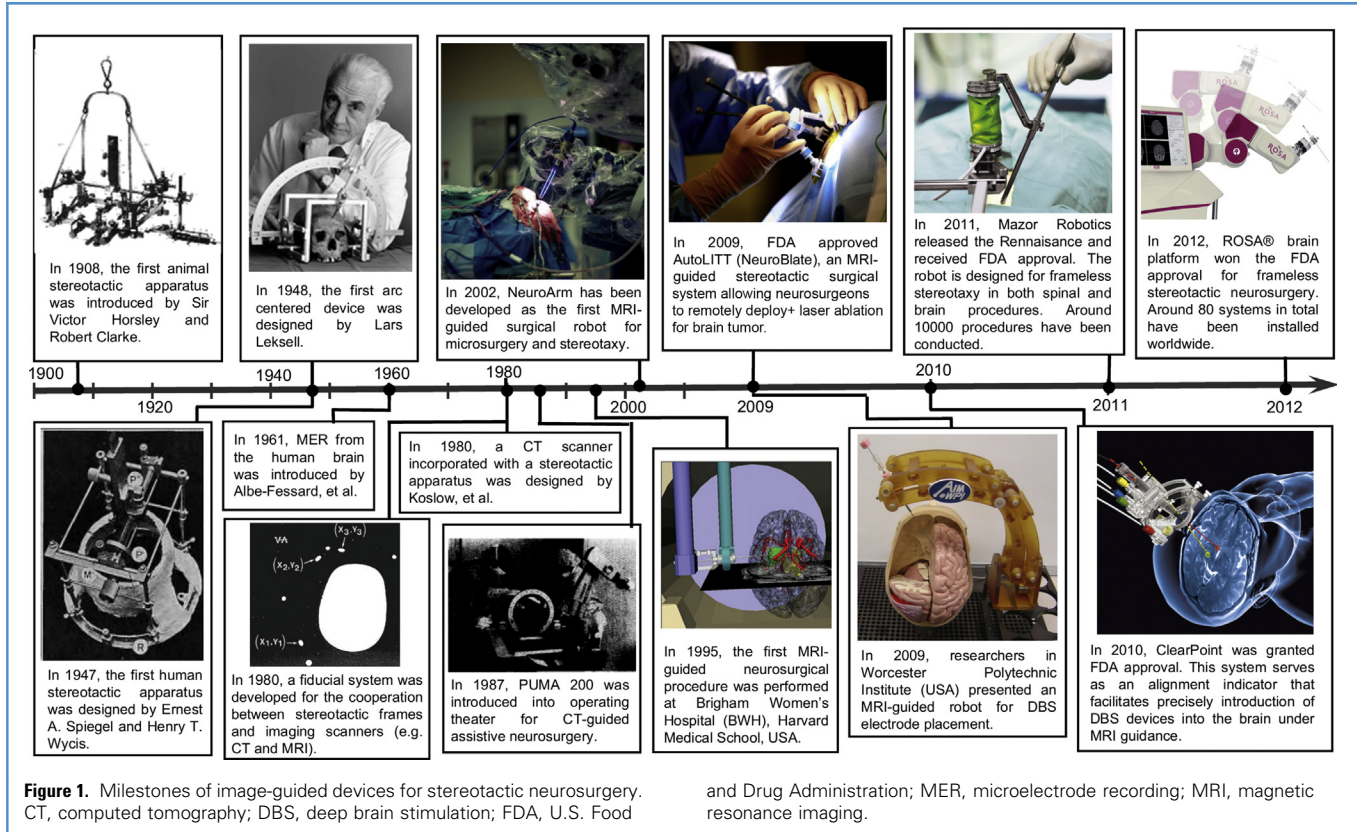
BACKGROUND

Stereotactic neurosurgery is a technique that can locate targets of interest within the brain using a three-dimensional (3D) coordinate system.[1] Stereotactic approaches have been widely used in a variety of procedures, such as biopsy, injection, ablation, catheter placement, stereoelectroencephalography, and deep brain stimulation (DBS). The current workflow for stereotaxy comprises 3 primary stages: 1) preoperative planning, which requires imaging conducted before operation; computed tomography (CT) and/or magnetic resonance (MR) imaging (MRI) (e.g., gadolinium-enhanced volumetric MRI) are the 2 common imaging modalities that can offer precise lesion localization, in targeting of deep brain structures for treatment of functional disorders, MRI is advantageous in visualizing

tissue such as deep brain nuclei in high tissue resolution and evaluating these structures with functional imaging techniques; 2) immediate planning with frame, which is a stage involving 3D coordinates registration between the images and the stereotactic frame; image fusion is commonly adopted in this step, in which CT images are usually fused with preoperative MRI for surgical planning; 3) intraoperative refinement, which includes setting up the platform for the coordinates and trajectory; a burr hole and dural puncture are made. Conventional stereotaxy for DBS includes microelectrode recording and macrostimulation for physiologic validation.

Despite the standard workflow that has been established for decades, stereotactic surgery still remains challenging, particularly because of the high demand for precision and minimal invasiveness. Imprecise positioning of instruments

results in a deviated trajectory and targeting error, which significantly increases the risk of hemorrhage. In the current workflow, several strategies are used to limit the error.[2,3] Patients are positioned in a similar way to the scanning position. During surgery, brain shift can be reduced in several ways. Minimal cerebrospinal fluid can be achieved by 1) placing the 14-mm burr hole and a small dural opening (3—4 mm) on a gyrus rather than a sulcus, 2) flooding the burr hole with saline irrigation after dural opening, and 3) sealing the dural defect with fibrin glue as soon as the electrode is in situ and before test stimulation. However, these strategies still cannot compensate for the changing conditions during surgery without continuous updates of instrument position relative to the target. Registration (image fusion) at the planning stage may provide only a 1-time calibration for the surgical roadmap based on the preoperative images. Errors

Figure 1. Milestones of image-guided devices for stereotactic neurosurgery. CT, computed tomography; DBS, deep brain stimulation; FDA, U.S. Food and Drug Administration; MER, microelectrode recording; MRI, magnetic resonance imaging.

can still come from various sources: 1) lead time between scanning and surgery; 2) mechanical error of the frame; 3) number of sampling fiducial points for registration; and 4) intrinsic error in image fusion. Once the dura is opened, brain shift/deformation inevitably causes changes of both critical brain structures and target positions. During surgery, brain deformation occurs in response to many factors of surgical manipulation and anesthesia procedures such as intracranial pressure changes, postural and gravitational forces, tissue removal, administration of pharmaceuticals, and edema caused by surgery. Therefore, using only preoperative images to form the roadmap seems to be the major disadvantage in the current workflow for stereotaxy.

In the context of current neurosurgical challenges, the incorporation of advances in real-time visualization and precise manipulation is imminent for brain shift compensation and workflow simplification. MRI possesses several advantages over other imaging modalities (e.g., ultrasonography or CT) for intraoperative guidance, because of its high sensitivity to intracranial pathologic/physiologic changes and ability to visualize soft tissue in high-contrast images without ionizing radiation. Fast MRI sequences (such as radial fast imaging using low angle shot sequence with a temporal resolution of 20–30 milliseconds[4]) have been widely available in MRI facilities and have already enabled surgical guidance when involving soft tissue deformation. The field is ready for an MRI-guided robot to find its way into more complex procedures, which would provide precise stereotactic guidance to deliver image-guided therapy, such as device implantation or tissue ablation. In this review, we provide a discussion regarding the state-of-the-art apparatus and MRI-safe/conditional robots for stereotactic neurosurgery, as well as the key enabling techniques with emphasis on their status, limitations, and future trends.

NEEDS FOR CURRENT APPARATUS AND MRI-GUIDED ROBOTIC SYSTEMS

The introduction of computer-based image navigation systems has allowed intraoperative guidance based on preoperative images since the 1990s (the evolution of devices in stereotactic neurosurgery is shown in **Figure 1**).[5] These advances in both imaging and tracking technologies enable frameless stereotaxy to be increasingly used. Frameless techniques use landmarks (e.g., facial contours) or fiducial markers to replace the frame for registration between images and operation space. Particularly, its incorporation with intraoperative MRI guidance can optimize the procedure by providing real-time positional information of imaged brain/surgical instruments, compensating brain shift, reducing registration errors, monitoring surgical progress, and performing MRI-based verification instead of physiologic assessment for DBS.[6,7]

Several clinical trials have been conducted using manually operated MR-safe/conditional stereotactic platforms (e.g., NexFrame [Medtronic Inc., Minneapolis, Minnesota, USA] and SmartFrame [ClearPoint, MRI Interventions Inc., Irvine, California, USA].[3,8-10] The ClearPoint system (**Figure 2A**) has been deployed in several therapeutic approaches (e.g.,
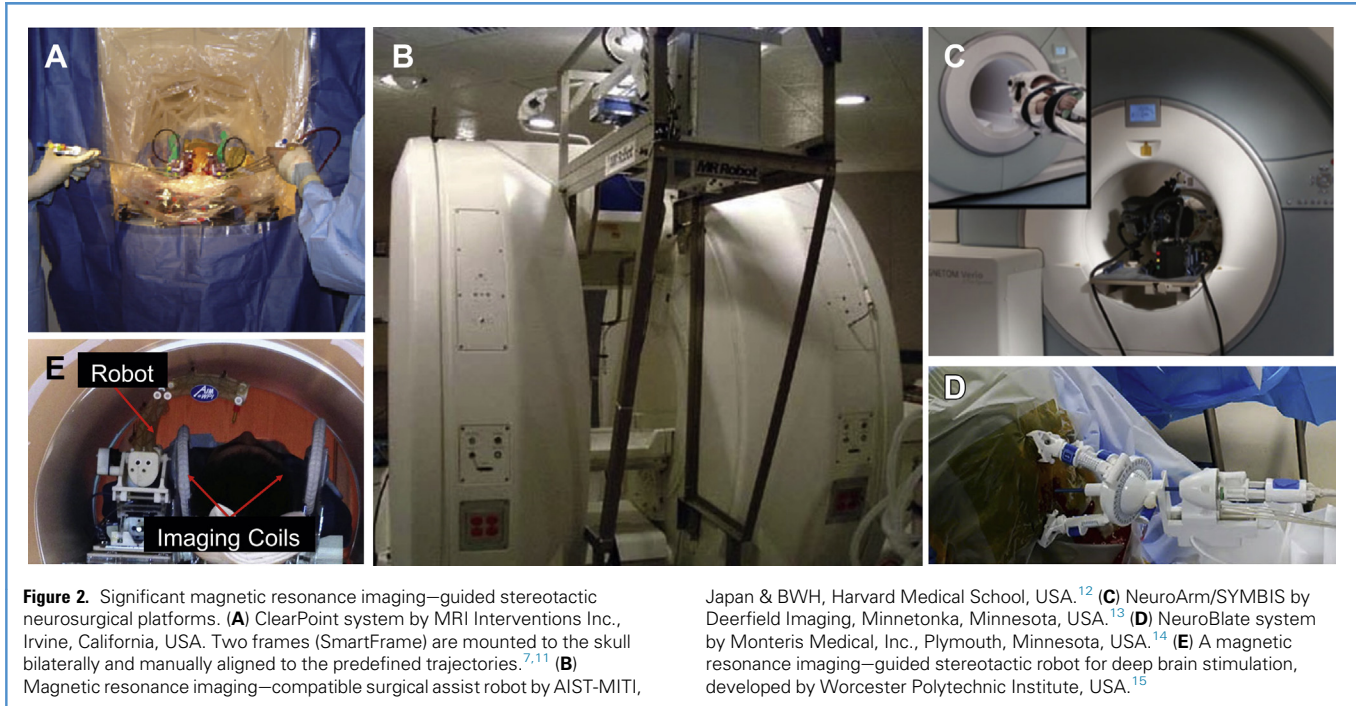
Figure 2. Significant magnetic resonance imaging—guided stereotactic neurosurgical platforms. (**A**) ClearPoint system by MRI Interventions Inc., Irvine, California, USA. Two frames (SmartFrame) are mounted to the skull bilaterally and manually aligned to the predefined trajectories.[7,11] (**B**) Magnetic resonance imaging—compatible surgical assist robot by AIST-MITI, Japan & BWH, Harvard Medical School, USA.[12] (**C**) NeuroArm/SYMBIS by Deerfield Imaging, Minnetonka, Minnesota, USA.[13] (**D**) NeuroBlate system by Monteris Medical, Inc., Plymouth, Minnesota, USA.[14] (**E**) A magnetic resonance imaging—guided stereotactic robot for deep brain stimulation, developed by Worcester Polytechnic Institute, USA.[15]

electrode placement,[16] focal ablation,[17] and direct drug delivery[18]). A clinical study[19] was performed using the ClearPoint system in DBS for 27 adult patients with movement disorder. All procedures were performed with interventional MRI scanners (1.5 and 3 T), and patients could be moved between the isocenter and the bore edge. The aiming device (SmartFrame) could be adjusted to the intended trajectory by surgeons remotely, when the patient was at the isocenter. In this study, no case required more than 2 passes. The radial errors observed were 0.68 ± 0.42 mm (1.5-T procedures) and 0.78 ± 0.38 mm (3-T procedures). The procedure duration was counted between the initial skin incision and final skin closure. It was approximately 3.5—4 hours for bilateral procedures, 217.1 ± 33.3 minutes (1.5-T procedures), and 247.6 ± 44.7 minutes (3-T procedures). Another single-center study[20] reported the clinical outcomes of using the ClearPoint system for bilateral DBS therapy. Twenty-six patients with advanced Parkinson disease and motor fluctuations were enrolled, and 20 patients were followed for 12 months. Symptom severity was evaluated using the change in Unified Parkinson's Disease Rating Scale

Part III off-medication score as the primary outcome variable. The mean Unified Parkinson's Disease Rating Scale Part III off-medication score was improved from 40.75 ± 10.9 to 24.35 ± 8.8 ($P = 0.001$). On-medication time without troublesome dyskinesia increased 5.2 ± 2.6 hours per day ($P = 0.0002$). Mean targeting error was 0.6 ± 0.3 mm.

However, the procedures can still be complicated and time-consuming. Patients need to be transferred between the operating room and MRI suite for scanning/manual manipulation (e.g., needle insertion), which greatly increases the operation time and disrupts the surgical rhythm. In addition, these systems still require the meticulous attention of surgeons to detail the hardware application. These challenges have directed increasing attention to the development of remotely controlled manipulators and further facilitate the translation of robotics technology into neurosurgery. Robots have superior capabilities over humans in certain tasks, especially in those that are demand accuracy and are space limited, exhaustive, and repetitive. The clinical benefits have been shown in the recent surge of robot-assisted surgical interventions.[21-23]

The first MRI-compatible manipulator toward stereotactic neurosurgical applications was built by Masamune et al.[24] and tested in vitro. Chinzei et al.[12,25] developed a surgical assist robot (**Figure 2B**) based on a low-field interventional scanner (i.e., Signa SP 0.5T [GE Medical Systems, Boston, Massachusetts, USA]). It is the first to be integrated with an optically linked frameless stereotactic tracking system.[26] However, surgeons have to operate inside the MRI room. The confined workspace of interventional MRI may affect their performance, especially during long and complicated operations. Moreover, the use of open or large bore scanners often comes with the sacrifice of image quality. This imaging can be further degraded by the metallic components used in the robot.

NeuroArm/SYMBIS surgical system (Deerfield Imaging, Minnetonka, Minnesota, USA) is an MRI-compatible robotic system for teleoperated microsurgery and stereotactic brain biopsy.[27,28] It consists of two 7+1 degrees of freedom (DoFs) manipulators semi-actively controlled by a remote workstation.[29] Hand tremor filter, movement scaling, and augmented force feedback are adopted. Microsurgery is generally performed by these 2

Table 1. Existing Robotic Systems for Magnetic Resonance Imaging—Guided Neurosurgery
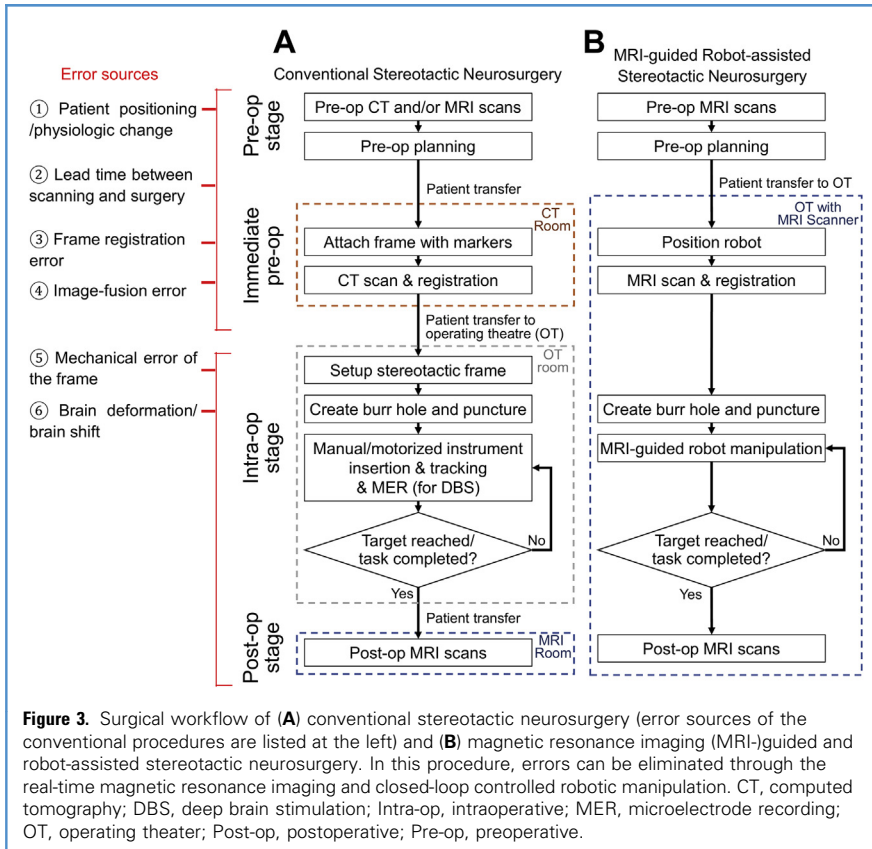
Emerging Platforms	Degree of Freedom	Number of End Effector	Actuator*	Accuracy	Human—Machine Interface	Features	Key References
NeuroArm/SYMBIS (Deerfield Imaging, Minnetonka, Minnesota, USA)	7+1	2	E	Submillimeter	√	Teleoperated microsurgery and stereotaxy; only 1 manipulator can fit into the magnet bore; haptic feedback; three-dimensional image reconstruction for navigation; phase: FDA approved, commercial	Sutherland et al., 2003[35]; Louw et al., 2004[36]; Motkoski et al., 2016[13]
NeuroBlate (Monteris Medical, Inc., Plymouth, Minnesota, USA)	2	1	E	1.57 ± 0.21 mm	√	Laser ablation; patient under general anesthesia; continuous MR thermography acquisition; phase: FDA approved, commercial	Mohammadi et al., 2014[33]; Manijila et al., 2016[37]
Pneumatic MRI-compatible needle driver (Vanderbilt University, USA)	2	1	P	1.11 mm	—	Transforaminal ablation; precurved concentric tube; 3-T closed-bore MRI scanner; phase: clinical trial	Comber et al., 2016[38]; Comber et al., 2016[39]
MRI-guided surgical manipulator (AIST-MITI, Japan & BWH, Harvard University, USA)	5	1	E	0.17 mm/0.17°	—	Navigation and axisymmetric tool placement; 0.5-T open MRI scanner; pointing device only; phase: in vivo test with a swine brain	Chinzei et al., 2001[25]; Koseki et al., 2004[40]
MRI-compatible stereotactic neurosurgery robot (Worcester Polytechnic Institute, USA)	7	1	E	1.37 ± 0.06 mm	—	Needle-based neural interventions; mounted at the MRI table; SNR reduction in imaging <10.3%; phase: research prototype	Li et al., 2015[15]; Nycz et al., 2017[34]
Mesoscale neurosurgery robot (Georgia Institute of Technology, USA)	†	1	‡	About 1 mm	—	Tumor resection, intracerebral hemorrhage evacuation; skull-mounted; phase: research prototype	Ho et al., 2015[41]; Kim et al., 2017[42]; Cheng et al., 2017[43]
MR-safe bilateral stereotactic robot (The University of Hong Kong, Hong Kong)	8	2	H	1.73 ± 0.75 mm	—	Bilateral stereotactic neurosurgery; skull-mounted; MR-safe/induce minimal imaging interference (SNR reduction ≤2.5%); phase: research prototype	Guo et al., 2018[44]
Multi-imager compatible needle-guide robot (Johns Hopkins University, USA)	3	1	P	1.55 ± 0.81 mm	—	General needle-based interventions; table-mounted; intraoperative MRI scanner (iMRIS); phase: research prototype	Jun et al., 2018[45]
MRI-compatible needle insertion manipulator (University of Tokyo, Japan)	6	1	E	3.0 mm	—	Needle placement; 0.5-T MRI scanner; phase: research prototype	Masamune et al., 1995[24]; Miyata et al., 2002[46]
Endoscope manipulator (AIST, Japan)	4	1	E	About 0.12 mm/0.04°	—	Endoscope manipulation for transnasal neurosurgery; vertical field open MRI; large imaging noise caused by ultrasonic motors; phase: research prototype	Koseki et al., 2002[47]
Telerobotic system for MRI-guided neurosurgery (California State University, USA & University of Toronto, Canada)	7	1	P/H	—	√	Brain biopsy; 1.5-T MRI scanner; mounted at the surgical table; phase: research prototype	Raoufi et al., 2008[48]
Open MRI compatible robot (Beihang University, China)	5	1	E	—	—	Biopsy and brachytherapy; 0.3-T intraoperative MRI scanner; phase: research prototype	Hong et al., 2008[49]

FDA, Food and Drug Administration; MR, magnetic resonance; MRI, magnetic resonance imaging; SNR, signal-to-noise ratio.
*Actuator: E, nonmagnetic electric actuator, such as piezoelectric motor or ultrasonic motor; P, pneumatic actuator; H, hydraulic actuator.
†A flexible continuum robot, of which the degrees of freedom depend on the number of segments.
‡Shape memory alloy spring-based actuators remotely driving the manipulator via pulling tendons.

Figure 3. Surgical workflow of (**A**) conventional stereotactic neurosurgery (error sources of the conventional procedures are listed at the left) and (**B**) magnetic resonance imaging (MRI-)guided and robot-assisted stereotactic neurosurgery. In this procedure, errors can be eliminated through the real-time magnetic resonance imaging and closed-loop controlled robotic manipulation. CT, computed tomography; DBS, deep brain stimulation; Intra-op, intraoperative; MER, microelectrode recording; OT, operating theater; Post-op, postoperative; Pre-op, preoperative.

manipulators outside the magnet bore, whereas stereotaxy is conducted within the bore using a single MRI-compatible robotic arm. This arm is directly attached to the magnet bore (Figure 2C) to provide a constant spatial relationship with the isocenter of the magnet and therefore the patient's disease.[13] A study of the NeuroArm system used in 56 patients was reported,[27] primarily for the treatment of central nervous system neoplasia and cavernous angioma. A case study showed that the total duration of glioma surgery was about 33 minutes excluding craniotomy and wound closure. In another clinical study,[13] 22 patient cases were treated using the NeuroArm, involving 10 meningioma, 9 glioma, 2 acoustic schwannoma, and 1 brain abscess. All procedures required general anesthetic and craniotomy. After partial dissection of the disease, the NeuroArm system was then brought into the surgical field. Working at the master console, surgeons were able to telemanipulate tools within the small surgical corridors, coagulate vessels to control bleeding, and aspirate.

The Monteris stereotactic platform (Figure 2D) is an MRI-based system for Minimally Invasive Robotic Laser Thermotherapy. It permits surgeons to remotely control the NeuroBlate laser probe (translation and rotation) driven by a 2-DoF piezomotor-actuated robotic device. The lasing portion at different directions can be planned and controlled via the computer workstation under MR thermography guidance, ensuring maximum coverage of the prescribed thermal injury.[30,31] This is a preferred feature for contoured ablation of irregular-shaped targets. Once ablation is complete on a given point/slice, the software can robotically advance the laser probe to the next location, begin MRI thermal imaging, plan ablation, then again rotate and fire the laser.[32] However, the orientation of the laser probe is fixed during the surgery by a separate stereotactic frame (AXiiiS stereotactic miniframe). Thus, patients requiring multiple trajectories may be transferred back to the operating room for probe removal, frame relocation/realignment, or possible drilling of a new burr hole.

Clinical outcomes using the NeuroBlate system for difficult-to-access high-grade gliomas were reported in a multicenter study.[33] It evaluated 24 patients with glioblastoma and 10 with anaplastic glioma who underwent laser interstitial thermal therapy (LITT) with a main focus on progression-free survival using precise volumetric analysis. LITT was delivered as upfront in 19 cases and as salvage in 16 cases. After 7.2 months follow-up, 71% of cases showed progression and 34% died. Median progression-free survival was 5.1 months. Thirteen cases met the following 2 criteria: 1) <0.05 cm³ tumor volume not covered by the 43°C-for-2-minutes thermal damage threshold line; 2) <0.15 cm³ tumor volume not covered by the 43°C-for-10-minutes thermal damage threshold line. Promising results showed LITT for patients with high-grade glioma was a safe and efficient treatment method.

A research prototype (Figure 2E) developed by Fischer et al.[15,34] was designed to perform needle-based neural interventions inside the MRI bore. The system features 7 DoFs driven by piezoelectric ultrasonic motors, in which a 2-DoF needle driver was recently implemented for rotating and inserting an interstitial ultrasound-based ablation probe.[34] The robot mechanism is based on the functionality and kinematic structure of the conventional stereotactic frame (e.g., Leksell frame). A laboratory-based study reported its accuracy of 1.37 ± 0.06 mm in tip position and 0.79° ± 0.41° in orientation.[34] However, the signal-to-noise ratio reduction in imaging reached 10.3% when the needle driver was running. Enhanced shielding of cables and direct current power lines of robot may be essential to improve the imaging quality and obviate relevant concerns before its next stage of development.

KEY ENABLING TECHNOLOGIES OF MRI-GUIDED ROBOTIC SYSTEMS

Despite the emergence of many MRI-guided neurosurgical robotic systems (as listed in Table 1), only a few are in widespread clinical use. The common technical challenges in conjunction with the use of robotics in MRI include MRI compatibility, manipulation within the confined workspace of scanner bore, real-time imaging with sufficient quality for

targets/instruments localization, and navigation. Most previous studies addressed only part of these challenges and still did not significantly improve the surgical workflow, in which longer procedure time (i.e., with frequent patient transfers) probably leads to high costs. The surgical costs for patients could also involve MRI scans, the use of robot/MRI-compatible instruments, and the extra labor for robot operation.[50] This high cost may be the vital factor that restricts the wide application of robotics technology in health care.[51] We propose 3 key enabling technologies for high-performance intraoperative MRI-guided robotic platforms. It may simplify the workflow as shown in **Figure 3B** and potentially reduce the surgical costs. Microelectrode recording and/or macrostimulation for DBS are still technically possible in our proposed procedure if the patient is awake.

Intraoperative Image Registration for Real-Time Stereotactic Planning

Image registration enables precise localization of the preoperatively segmented

critical/target regions on the rapidly acquired intraoperative image to establish/update the stereotactic guidance accordingly. Many commercial navigation systems use only rigid registration to realign both sets of images. However, it cannot compensate for any nonlinear image discrepancy resulting from brain deformation and MRI distortion (e.g., severe misalignment [$\sim$10−30 mm[52]]) caused by brain shift after craniotomy (**Figure 4**). Thus nonrigid image registration has been proposed to mitigate such nonlinear misalignment. In particular, biomechanical finite-element−based registration schemes are developed to estimate and predict the extension of any brain shift of different regions.[53,55,56]

Apart from nonlinear image discrepancy caused by tissue deformation, spatial distortion of MRIs would also hamper the accuracy in MRI-guided stereotactic surgery.[57] The cause of MR distortion is multiform and incalculable. Aside from base (static) field inhomogeneity, chemical shift, and susceptibility artifacts, the nonlinearity of the B1

gradient field contributes most to such distortion. It has been reported that the spatial distortion can be as much as 25 mm at the perimeter of an uncorrected 1.5-T MRI, with the error still remaining within the 1% range (typically $\sim$4 mm) even after correction using standard gradient calibration (e.g., grid phantoms).[58,59] This error is significant regarding the stringent accuracy requirement in stereotaxy. Worse still, the distortion is exacerbated under higher magnetic field inhomogeneity that presents in 3-T scanners.[57] The combined effect of these variables often results in complex and nondeterministic image distortion.[60]

Considering such gradient field nonlinearity, gradient-based excitation sequences were set back despite its widespread usefulness. Nonrigid registration schemes can correct the distortion in a gradient-based image and retain any useful anatomic information, by registering the distorted image to a standard MRI (e.g., T2 turbo spin echo images, which show few image distortions). Recent research has shown that significant (>10%) improvement in accuracy has been achieved by resolving such misalignment.[61] However, complex computation involved in nonrigid registration may impede its efficacy when used in intraoperative scenarios. This factor motivates the development of high-performance registration schemes using scalable computation architectures such as graphic processing units, field-programmable gate arrays, or computational clusters. Recent studies[62-65] have shown substantial computation speed-up, in which the registration process can be accomplished within seconds, even with a large data set in a 3D image ($\sim$27 M voxels).

MR-Based 3D Positional Tracking of Stereotactic Instruments

Real-time tracking provides in situ positional feedback of stereotactic instruments inside the MRI scanner. Not only does it act as feedback data to close the control loop of a robotic system, it also allows the operator to visualize the instrument position/configuration with reference to the brain roadmap. Restricted space inside the scanner bore and complicated electromagnetic (EM) shielding have limited
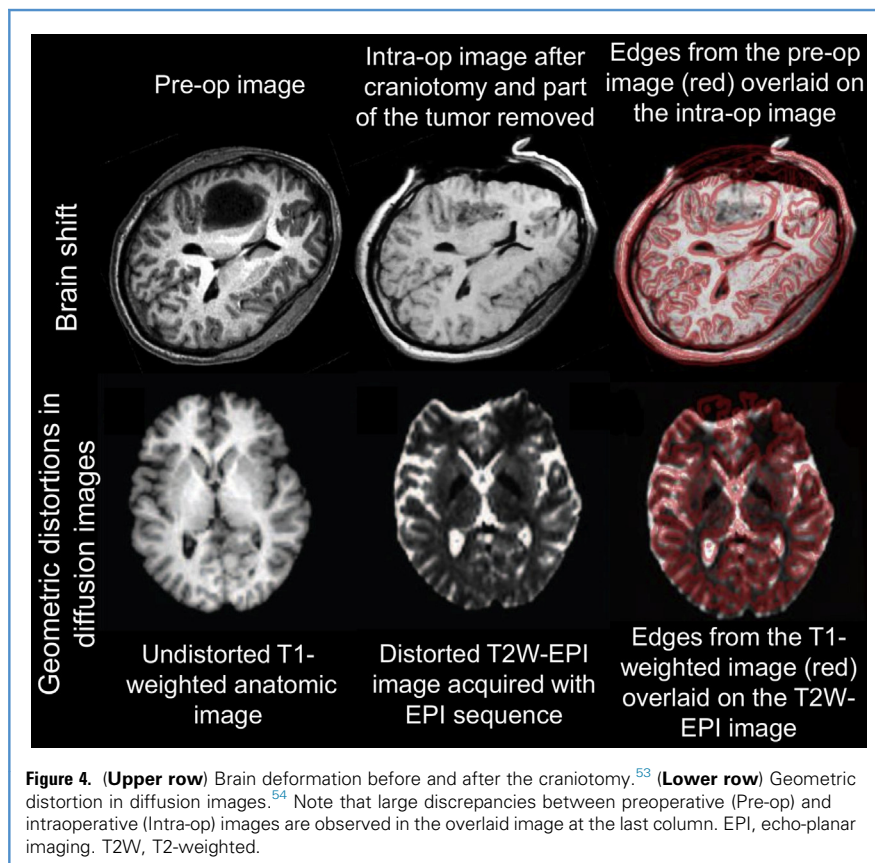

Figure 4. (**Upper row**) Brain deformation before and after the craniotomy.[53] (**Lower row**) Geometric distortion in diffusion images.[54] Note that large discrepancies between preoperative (Pre-op) and intraoperative (Intra-op) images are observed in the overlaid image at the last column. EPI, echo-planar imaging. T2W, T2-weighted.
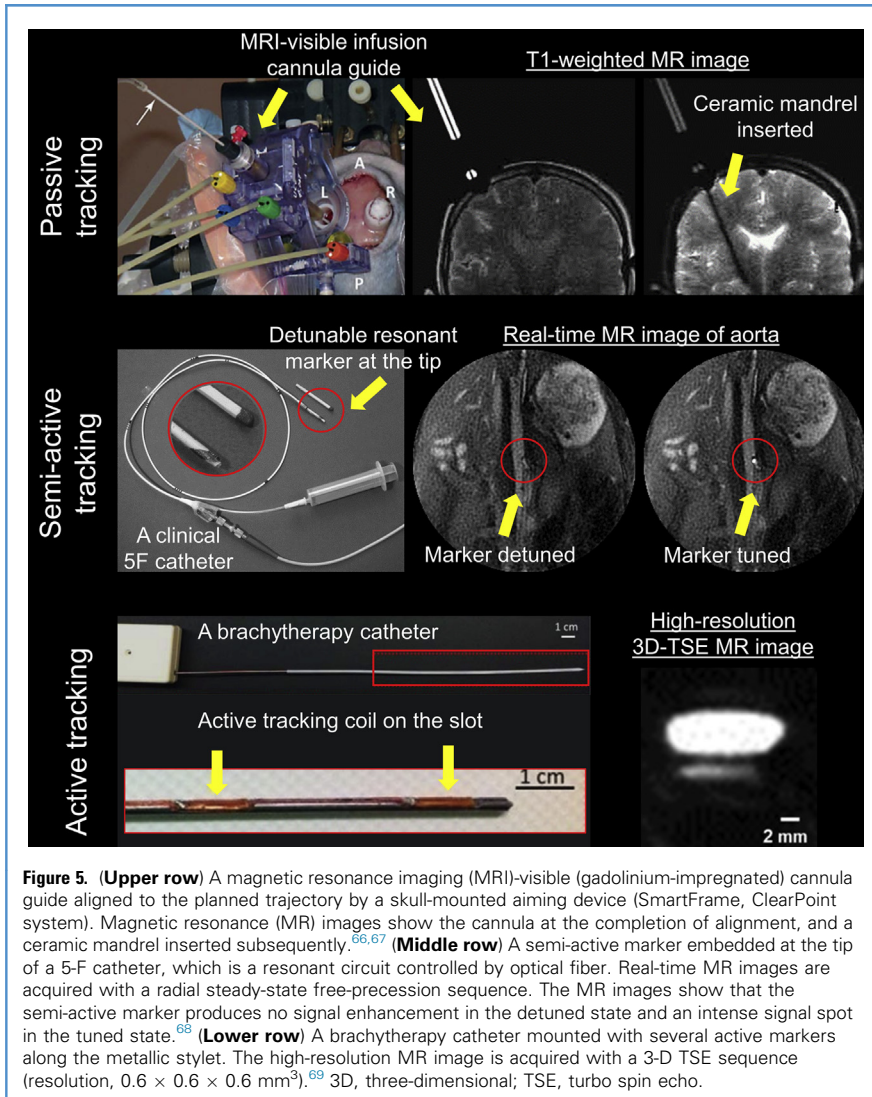
Figure 5. (**Upper row**) A magnetic resonance imaging (MRI)-visible (gadolinium-impregnated) cannula guide aligned to the planned trajectory by a skull-mounted aiming device (SmartFrame, ClearPoint system). Magnetic resonance (MR) images show the cannula at the completion of alignment, and a ceramic mandrel inserted subsequently.[66,67] (**Middle row**) A semi-active marker embedded at the tip of a 5-F catheter, which is a resonant circuit controlled by optical fiber. Real-time MR images are acquired with a radial steady-state free-precession sequence. The MR images show that the semi-active marker produces no signal enhancement in the detuned state and an intense signal spot in the tuned state.[68] (**Lower row**) A brachytherapy catheter mounted with several active markers along the metallic stylet. The high-resolution MR image is acquired with a 3-D TSE sequence (resolution, 0.6 × 0.6 × 0.6 mm³).[69] 3D, three-dimensional; TSE, turbo spin echo.

projection.[74] This localization is automatic, because the marker can be independently identified through its own receiving channel.[75,76] However, resonating radiofrequency waves and electric energy stored in conductive structures may induce heat and require delicate control.[77] In light of this complication, semi-active tracking systems without any electric wiring connected to the scanner have been developed (**Figure 5**, middle row).[78] This wireless marker acts as a radiofrequency receiver to pick up the MR gradient signal, as well as an inductor to resonate with the signal transmitted to the scanner receiver.[78] We can foresee that these MR-based tracking coils could be implemented in stereotactic neurosurgery to realize real-time instrument tracking. Promising results have been reported in an MR-active tracking system for MRI-guided brachytherapy. Three active microcoil markers (1.5 × 8 mm², **Figure 5**) are mounted on a brachytherapy stylet (with diameter of Ø1.6 mm).[69] Both tracking and imaging are in the same coordinate system, so the stylet configuration can be virtually augmented on MRIs in situ. Stylet localization could be achieved with low latency <1.5 milliseconds at high resolution (0.6 × 0.6 × 0.6 mm³) and a high sampling rate of 40 Hz.

MRI-Compatible Actuation for Precise Robot Manipulation

Safety and accuracy are particularly demanding for instrument manipulation in stereotactic neurosurgery, which involves precise coordination of at least 2 DoFs (e.g., rotation and insertion) and requires an average accuracy within 2 mm. The underlying actuators are a determinant component regarding the performance of robotic manipulation. The strong magnetic field generated by MRI scanners prevents the use of conventional high-performance EM-powered actuators. This situation poses a strong incentive to develop motors that are safe and compatible with the MRI environment. Nonmagnetic electric actuation (e.g., piezoelectric/ultrasonic motors powered by high-frequency electric current) have been extensively applied for interventional MRI applications.[79-81] Such motors are usually small (e.g., 40.5 × 25.7 × 12.7 mm³, nanomotion motor; **Figure 6**, upper row),

the application of external tracking devices (e.g., stereo-optical cameras). Passive tracking (**Figure 5**, upper row) is the most commonly used technique. It can be adopted under various MR field strengths. Passive markers (e.g., capsulized fish oil and vitamin E) incorporated with the stereotactic instruments are visible in MRIs by changing the image contrast. Generally, the configuration of marker system needs to be specially designed for ready identification,[70] otherwise it may be invalid when markers are in proximity or out of the imaging slice.[71] However, it is still challenging to perform localization of passive markers automa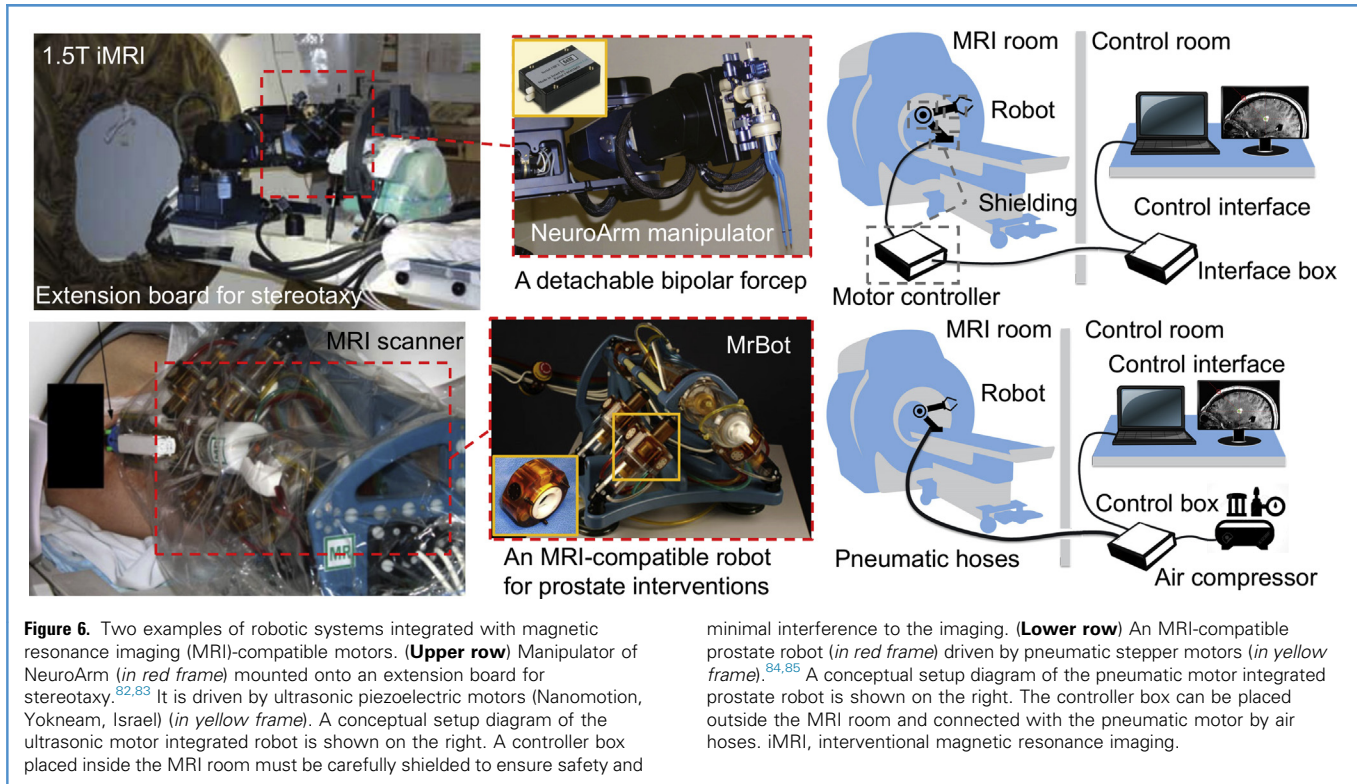tically in real time. The visualization of these markers relies on 2D image reconstruction. This process is time-consuming (e.g., 9.440 seconds[72] required for acquisition of 1 T2-weighted MRI slice with field of volume of 220 × 220 mm²) and may not be reliable because of the intrinsically distorted MRIs.[73]

To resolve the problems in passive tracking, much research attention has recently been drawn to MR-based tracking techniques. An active marker (**Figure 5**, lower row) is a small coil individually connected with the scanner receiver. It serves as an antenna and actively responds to the MR gradient field along 3 principal directions. Without image reconstruction, they can be rapidly localized using one-dimensional

Figure 6. Two examples of robotic systems integrated with magnetic resonance imaging (MRI)-compatible motors. (**Upper row**) Manipulator of NeuroArm (*in red frame*) mounted onto an extension board for stereotaxy.[82,83] It is driven by ultrasonic piezoelectric motors (Nanomotion, Yokneam, Israel) (*in yellow frame*). A conceptual setup diagram of the ultrasonic motor integrated robot is shown on the right. A controller box placed inside the MRI room must be carefully shielded to ensure safety and minimal interference to the imaging. (**Lower row**) An MRI-compatible prostate robot (*in red frame*) driven by pneumatic stepper motors (*in yellow frame*).[84,85] A conceptual setup diagram of the pneumatic motor integrated prostate robot is shown on the right. The controller box can be placed outside the MRI room and connected with the pneumatic motor by air hoses. iMRI, interventional magnetic resonance imaging.

and can provide fine movement at the nanoscale. However, the EM interference is inevitably induced by the high-frequency electric signals. Tailor-made EM shielding[80,86] of motors and their electronic drivers may alleviate this interference, but the imaging quality is more or less deteriorated. Such motors may not operate during image acquisition or be placed near the target of interest (e.g., small DBS targets with diameter of $\varnothing 4-12$ mm).

As a result, motors powered by intrinsically MR-safe energy sources (e.g., pressurized air/water flow) have been developed.[84,87-90] This fluid-driven actuation usually generates only minimal EM interference and unobservable image artifacts. **Figure 6** shows a general setup of a pneumatically actuated MRI robot. Long transmission pipes (e.g., 10 m) connect the robot with its control box, which are placed in the MRI and control rooms, respectively. Through such long transmission, torque/force outputs of air motors are usually limited as a result of the air compressibility. Also, it is difficult to reach millimeter level for positional accuracy as required in

stereotaxy.[91] In addition, air might not be tightly sealed and would be allowed to exhaust into the atmosphere, which would generate unfavorable noise and vibration.

In contrast, incompressible liquid (e.g., water and oil) in hydraulic motors may offer relatively high-performance mechanical transmission. They can typically render large power, as well as more accurate and responsive positional output. A common concern of using hydraulics is the discreet management of liquid leakage. Recent advances in sealing methods[92,93] (e.g., rolling diaphragm-sealed) may offer reliable solutions and be readily translated into MR-safe actuation. The other constraint of hydraulic motors is their bulky size and the restricted workspace spared by the MRI head coil. Remote transmission between manipulator and actuator may tackle this problem by separately settling the actuation unit at a surgical table. For example, in the ClearPoint system (**Figure 2A**), 4 semi-rigid shafts connecting the trajectory guide and control knobs can transmit remote manipulation with submillimeter accuracy.[7] The results indicate the

promising incorporation of this remote actuation method in an MRI robot, enabling the use of high-performance hydraulic motors and also greatly reducing the weight/dimension of manipulators.

CONCLUSIONS

In this review, we have provided an outline of the emerging robotic platforms for MRI-guided stereotactic neurosurgery. Various robotic systems are introduced, allowing for enhanced dexterity, stability, and accuracy beyond manual operation. However, few are widely adopted. This situation may be because of the lack of effectiveness to compensate the high cost, including MRI scanning, use of MRI-compatible instruments/robot, and extra labor. To simplify the workflow and potentially enhance surgical outcomes, 3 key enabling techniques have been discussed, namely image registration, positional tracking, and MRI-compatible actuation. Because brain shift and MRI distortion are inevitable, nonrigid image registration may prove to be essential in future navigation systems. MR-based tracking can provide real-time positional

data with high resolution and update rate. It would allow reliable online 3D tracking of stereotactic instruments. Hydraulic motors can contribute to precise manipulation by offering high-performance actuation under MRI, without adversely affecting the imaging quality. All technological developments will serve to exploit the information available and augment the surgeon's abilities by providing enhanced visualization and manipulation. Continued efforts to incorporate these techniques and to evaluate the clinical benefits would be invaluable in the progression of MRI-guided robot-assisted stereotactic neurosurgery.

REFERENCES

1. Galloway R, Maciunas RJ. Stereotactic neurosurgery. *Crit Rev Biomed Eng.* 1989;18:181-205.

2. Zrinzo L. Pitfalls in precision stereotactic surgery. *Surg Neurol Int.* 2012;3(suppl 1):S53.

3. Foltynie T, Zrinzo L, Martinez-Torres I, Tripoliti E, Petersen E, Holl E, et al. MRI-guided STN DBS in Parkinson's disease without microelectrode recording: efficacy and safety. *J Neurol Neurosurg Psychiatry.* 2011;82:358-363.

4. Uecker M, Zhang S, Voit D, Karaus A, Merboldt KD, Frahm J. Real-time MRI at a resolution of 20 ms. *NMR Biomed.* 2010;23:986-994.

5. Mert A, Gan LS, Knosp E, Sutherland GR, Wolfsberger S. Advanced cranial navigation. *Neurosurgery.* 2013;72:A43-A53.

6. Hadani M, Spiegelman R, Feldman Z, Berkenstadt H, Ram Z. Novel, compact, intra-operative magnetic resonance imaging-guided system for conventional neurosurgical operating rooms. *Neurosurgery.* 2001;48:799-809.

7. Chabardes S, Isnard S, Castrioto A, Oddoux M, Fraix V, Carlucci L, et al. Surgical implantation of STN-DBS leads using intraoperative MRI guidance: technique, accuracy, and clinical benefit at 1-year follow-up. *Acta Neurochir (Wien).* 2015;157:729-737.

8. Ashkan K, Blomstedt P, Zrinzo L, Tisch S, Yousry T, Limousin-Dowsey P, et al. Variability of the subthalamic nucleus: the case for direct MRI guided targeting. *Br J Neurosurg.* 2007;21:197-200.

9. Patel NK, Plaha P, Gill SS. Magnetic resonance imaging-directed method for functional neurosurgery using implantable guide tubes. *Neurosurgery.* 2007;61(suppl 5):ONS358-ONS366.

10. Larson P, Starr PA, Ostrem JL, Galifianakis N, Palenzuela MSL, Martin A. Application accuracy of a second generation interventional MRI stereotactic platform: initial experience in 101 DBS electrode implantations. *Neurosurgery.* 2013;60:187.

11. Starr PA, Markun LC, Larson PS, Volz MM, Martin AJ, Ostrem JL. Interventional MRI–guided deep brain stimulation in pediatric dystonia: first

experience with the ClearPoint system. *J Neurosurg Pediat.* 2014;14:400-408.

12. Chinzei K, Hata N, Jolesz FA, Kikinis R. MR compatible surgical assist robot: system integration and preliminary feasibility study. Paper presented at: International Conference on Medical Image Computing and Computer-Assisted Intervention. October 11-14, 2000; Berlin, Heidelberg, Germany. 921-930.

13. Motkoski JW, Sutherland GR. Why robots entered neurosurgery. *Exp Neurosurg Anim Models.* 2016: 85-105.

14. Golby AJ. *Image-Guided Neurosurgery.* Netherlands: Elsevier Science; 2015.

15. Li G, Su H, Cole G, Shang W, Harrington K, Camilo A, et al. Robotic system for MRI-guided stereotactic neurosurgery. *IEEE Trans Biomed Eng.* 2015;62:1077-1088.

16. Sidiropoulos C, Rammo R, Merker B, Mahajan A, LeWitt P, Kaminski P, et al. Intraoperative MRI for deep brain stimulation lead placement in Parkinson's disease: 1 year motor and neuropsychological outcomes. *J Neurol.* 2016;263:1226-1231.

17. Drane DL, Loring DW, Voets NL, Price M, Ojemann JG, Willie JT, et al. Better object recognition and naming outcome with MRI-guided stereotactic laser amygdalohippocampotomy for temporal lobe epilepsy. *Epilepsia.* 2015;56:101-113.

18. Chittiboina P, Heiss JD, Lonser RR. Accuracy of direct magnetic resonance imaging-guided placement of drug infusion cannulae. *J Neurosurg.* 2015; 122:1173-1179.

19. Southwell DG, Narvid JA, Martin AJ, Qasim SE, Starr PA, Larson PS. Comparison of deep brain stimulation lead targeting accuracy and procedure duration between 1.5-and 3-Tesla interventional magnetic resonance imaging systems: an initial 12-month experience. *Stereotact Funct Neurosurg.* 2016;94:102-107.

20. Ostrem JL, Ziman N, Galifianakis NB, Starr PA, Luciano MS, Katz M, et al. Clinical outcomes using ClearPoint interventional MRI for deep brain stimulation lead placement in Parkinson's disease. *J Neurosurg.* 2016;124:908-916.

21. Missios S, Bekelis K, Barnett GH. Renaissance of laser interstitial thermal ablation. *Neurosurg Focus.* 2015;38:E13.

22. Gonzalez-Martinez J, Vadera S, Mullin J, Enatsu R, Alexopoulos AV, Patwardhan R, et al. Robot-assisted stereotactic laser ablation in medically intractable epilepsy: operative technique. *Neurosurgery.* 2014;10:167-173.

23. Chang SD, Main W, Martin DP, Gibbs IC, Heilbrun MP. An analysis of the accuracy of the CyberKnife: a robotic frameless stereotactic radiosurgical system. *Neurosurgery.* 2003;52:140-147.

24. Masamune K, Kobayashi E, Masutani Y, Suzuki M, Dohi T, Iseki H, et al. Development of an MRI-compatible needle insertion manipulator for stereotactic neurosurgery. *J Image Guid Surg.* 1995;1:242-248.

25. Chinzei K, Miller K. Towards MRI guided surgical manipulator. *Med Sci Monit.* 2001;7:153-163.

26. Lewin JS, Metzger A, Selman WR. Intraoperative magnetic resonance image guidance in neurosurgery. *J Magn Reson Imaging.* 2000;12:512-524.

27. Sutherland GR, Maddahi Y, Gan LS, Lama S, Zareinia K. Robotics in the neurosurgical treatment of glioma. *Surg Neurol Int.* 2015;6(suppl 1):S1.

28. Sutherland GR, McBeth PB, Louw DF. NeuroArm: an MR compatible robot for microsurgery. Paper presented at: International Congress Series, June, 2003: 504-508.

29. Faria C, Erlhagen W, Rito M, De Momi E, Ferrigno G, Bicho E. Review of robotic technology for stereotactic neurosurgery. *IEEE Rev Biomed Eng.* 2015;8:125-137.

30. Hawasli AH, Ray WZ, Murphy RK, Dacey RG Jr, Leuthardt EC. Magnetic resonance imaging-guided focused laser interstitial thermal therapy for subinsular metastatic adenocarcinoma: technical case report. *Neurosurgery.* 2011;70(suppl_2): onsE332-onsE338.

31. Mohammadi AM, Hawasli AH, Rodriguez A, Schroeder JL, Laxton AW, Elson P, et al. The role of laser interstitial thermal therapy in enhancing progression-free survival of difficult-to-access high-grade gliomas: a multicenter study. *Cancer Med.* 2014;3:971-979.

32. LaRiviere MJ, Gross RE. Stereotactic laser ablation for medically intractable epilepsy: the next generation of minimally invasive epilepsy surgery. *Front Surg.* 2016;3:64.

33. Mohammadi AM, Hawasli AH, Rodriguez A, Schroeder JL, Laxton AW, Elson P, et al. The role of laser interstitial thermal therapy in enhancing progression-free survival of difficult-to-access high-grade gliomas: a multicenter study. *Cancer Med.* 2014;3:971-979.

34. Nycz CJ, Gondokaryono R, Carvalho P, Patel N, Wartenberg M, Pilitsis JG, et al. Mechanical validation of an MRI compatible stereotactic neurosurgery robot in preparation for pre-clinical trials. Paper presented at: IEEE/RSJ International Conference on Intelligent Robots and Systems (IROS). September 24-28, 2017; Vancouver, Canada.

35. Sutherland GR, McBeth PB, Louw DF. NeuroArm: an MR compatible robot for microsurgery. *International Congress Series.* 2003;1256:504-508.

36. Louw DF, Fielding T, McBeth PB, Gregoris D, Newhook P, Sutherland GR, et al. Surgical robotics: a review and neurosurgical prototype development. *Neurosurgery.* 2004;54:525-537.

37. Manjila S, Knudson KE, Johnson C Jr, Sloan AE. Monteris AXiiiS stereotactic miniframe for intracranial biopsy: precision, feasibility, and ease of use. *Neurosurgery.* 2016;12:119-127.

38. Comber DB, Pitt EB, Gilbert HB, Powelson MW, Matijevich E, Neimat JS, et al. Optimization of curvilinear needle trajectories for transforamenal hippocampotomy. *Neurosurgery.* 2016;13:15-22.

39. Comber DB, Slightam JE, Gervasi VR, Neimat JS, Barth EJ. Design, additive manufacture, and

control of a pneumatic MR-compatible needle driver. *IEEE Trans Robot.* 2016;32:138-149.

40. Koseki Y, Kikinis R, Jolesz FA, Chinzei K. Precise evaluation of positioning repeatability of MR-compatible manipulator inside MRI, Paper presented at: International Conference on Medical Image Computing and Computer-Assisted Intervention. September 26-29, 2004; Berlin, Heidelberg, Germany.

41. Ho M, Kim Y, Cheng SS, Gullapalli R, Desai JP. Design, development, and evaluation of an MRI-guided SMA spring-actuated neurosurgical robot. *Int J Rob Res.* 2015;34:1147-1163.

42. Kim Y, Cheng SS, Diakite M, Gullapalli RP, Simard JM, Desai JP. Toward the development of a flexible mesoscale MRI-compatible neurosurgical continuum robot. *IEEE Trans Robot.* 2017;33: 1386-1397.

43. Cheng SS, Kim Y, Desai JP. New actuation mechanism for actively cooled SMA springs in a neurosurgical robot. *IEEE Trans Robot.* 2017;33: 986-993.

44. Guo Z, Dong Z, Lee K-H, Cheung CL, Fu HC, Ho JD-L, et al. Compact design of a hydraulic driving robot for intra-operative MRI-guided bilateral stereotactic neurosurgery. *IEEE Robot Autom Lett.* 2018;3:2515-2522.

45. Jun C, Lim S, Wolinsky J-P, Garzon-Muvdi T, Petrisor D, Cleary K, et al. MR safe robot assisted needle access of the brain: preclinical study. *J Med Rob Res.* 2018;3:1850003.

46. Miyata N, Kobayashi E, Kim D, Masamune K, Sakuma I, Yahagi N, et al. Micro-grasping forceps manipulator for MR-guided neurosurgery. *Med Image Comput Comput Assist Interv.* 2002;2002: 107-113.

47. Koseki Y, Washio T, Chinzei K, Iseki H. Endoscope manipulator for trans-nasal neurosurgery, optimized for and compatible to vertical field open MRI. *Med Image Comput Comput Assist Interv.* 2002;2002:114-121.

48. Raoufi C, Goldenberg AA, Kucharczyk W. Design and control of a novel hydraulically/pneumatically actuated robotic system for MRI-guided neurosurgery. *J Biomed Sci Eng.* 2008;1:68.

49. Hong Z, Yun C, Zhao L, Wang Y. Design and optimization analysis of open-MRI compatibile robot for neurosurgery. 2nd International Conference on Bioinformatics and Biomedical Engineering. iCBBE. 2008.

50. Dorward N, Paleologos T, Alberti O, Thomas D. The advantages of frameless stereotactic biopsy over frame-based biopsy. *Br J Neurosurg.* 2002;16: 110-118.

51. Mattei TA, Rodriguez AH, Sambhara D, Mendel E. Current state-of-the-art and future perspectives of robotic technology in neurosurgery. *Neurosurg Rev.* 2014;37:357-366.

52. Nimsky C, Ganslandt O, Hastreiter P, Fahlbusch R. Intraoperative compensation for brain shift. *Surg Neurol.* 2001;56:357-364.

53. Archip N, Clatz O, Whalen S, Kacher D, Fedorov A, Kot A, et al. Non-rigid alignment of pre-operative MRI, fMRI, and DT-MRI with intra-operative MRI for enhanced visualization and navigation in image-guided neurosurgery. *Neuroimage.* 2007;35:609-624.

54. Bhushan C, Haldar JP, Choi S, Joshi AA, Shattuck DW, Leahy RM. Co-registration and distortion correction of diffusion and anatomical images based on inverse contrast normalization. *Neuroimage.* 2015;115:269-280.

55. Škrinjar O, Nabavi A, Duncan J. Model-driven brain shift compensation. *Med Image Anal.* 2002;6: 361-373.

56. Hu J, Jin X, Lee JB, Zhang L, Chaudhary V, Guthikonda M, et al. Intraoperative brain shift prediction using a 3D inhomogeneous patient-specific finite element model. *J Neurosurg.* 2007; 106:164-169.

57. Tavares WM, Tustumi F, da Costa Leite C, Gamarra LF, Amaro E Jr, Teixeira MJ, et al. An image correction protocol to reduce distortion for 3-T stereotactic MRI. *Neurosurgery.* 2014;74:121-127.

58. Baldwin LN, Wachowicz K, Thomas SD, Rivest R, Fallone BG. Characterization, prediction, and correction of geometric distortion in 3T MR images. *Med Phys.* 2007;34:388-399.

59. Mallozzi R. *Geometric distortion in MRI.* The Phantom Laboratory Inc; 2015. Available at: https://static1.squarespace.com/static/538f4542e4b089582 27fd19d/t/55dce491e4b0f0c3127be533/1440539793949/Geometric%2BDistortion%2Bin%2BMRI%2B.pdf.

60. Walker A, Liney G, Metcalfe P, Holloway L. MRI distortion: considerations for MRI based radiotherapy treatment planning. *Australas Phys Eng Sci Med.* 2014;37:103-113.

61. Murgasova MK, Lockwood-Estrin G, Nunes RG, Malik S, Rutherford M, Rueckert D, et al. Distortion correction in fetal EPI using non-rigid registration with a Laplacian constraint. *IEEE Trans Med Imaging.* 2018;37:12-19.

62. Kwok K-W, Chow GC, Chau TC, Chen Y, Zhang SH, Luk W, et al. FPGA-based acceleration of MRI registration: an enabling technique for improving MRI-guided cardiac therapy. *J Cardiovasc Magn Reson.* 2014;16(suppl 1):W11.

63. Kwok K-W, Chen Y, Chau TC, Luk W, Nilsson KR, Schmidt EJ, et al. MRI-based visual and haptic catheter feedback: simulating a novel system's contribution to efficient and safe MRI-guided cardiac electrophysiology procedures. *J Cardiovasc Magn Reson.* 2014;16(suppl 1):O50.

64. Gu X, Pan H, Liang Y, Castillo R, Yang D, Choi D, et al. Implementation and evaluation of various demons deformable image registration algorithms on a GPU. *Phys Med Biol.* 2009;55:207.

65. Kwok K-W, Lee K-H, Chen Y, Wang W, Hu Y, Chow GC, et al. Interfacing fast multi-phase cardiac image registration with MRI-based catheter tracking for MRI-guided electrophysiological ablative procedures. *Am Heart Assoc.* 2014;130: A18568.

66. Richardson RM, Kells AP, Martin AJ, Larson PS, Starr PA, Piferi PG, et al. Novel platform for MRI-guided convection-enhanced delivery of therapeutics: preclinical validation in nonhuman primate brain. *Stereotact Funct Neurosurg.* 2011;89: 141-151.

67. Truwit C, Martin AJ, Hall WA. MRI guidance of minimally invasive cranial applications. In: Kahn T, Busse H, eds. *Interventional Magnetic Resonance Imaging.* Berlin: Springer; 2011:97-112.

68. Weiss S, Kuehne T, Brinkert F, Krombach G, Katoh M, Schaeffter T, et al. In vivo safe catheter visualization and slice tracking using an optically detunable resonant marker. *Magn Reson Med.* 2004; 52:860-868.

69. Wang W, Dumoulin CL, Viswanathan AN, Tse ZT, Mehrtash A, Loew W, et al. Real-time active MR-tracking of metallic stylets in MR-guided radiation therapy. *Magn Reson Med.* 2015;73:1803-1811.

70. Strother SC, Anderson JR, Xu X-L, Liow J-S, Bonar DC, Rottenberg DA. Quantitative comparisons of image registration techniques based on high-resolution MRI of the brain. *J Comput Assist Tomogr.* 1993;18:954-962.

71. Elayaperumal S, Plata JC, Holbrook AB, Park Y-L, Pauly KB, Daniel BL, et al. Autonomous real-time interventional scan plane control with a 3-D shape-sensing needle. *IEEE Trans Med Imaging.* 2014;33:2128-2139.

72. Chavhan GB, Babyn PS, Thomas B, Shroff MM, Haacke EM. Principles, techniques, and applications of T2-based MR imaging and its special applications. *Radiographics.* 2009;29:1433-1449.

73. Wang D, Strugnell W, Cowin G, Doddrell DM, Slaughter R. Geometric distortion in clinical MRI systems: Part I: evaluation using a 3D phantom. *Magn Reson Imaging.* 2004;22:1211-1221.

74. Dumoulin C, Souza S, Darrow R. Real-time position monitoring of invasive devices using magnetic resonance. *Magn Reson Med.* 1993;29:411-415.

75. Werner R, Krueger S, Winkel A, Albrecht C, Schaeffter T, Heller M, et al. MR-guided breast biopsy using an active marker: a phantom study. *J Magn Reson Imaging.* 2006;24:235-241.

76. Zimmermann H, Müller S, Gutmann B, Bardenheuer H, Melzer A, Umathum R, et al. Targeted-HASTE imaging with automated device tracking for MR-guided needle interventions in closed-bore MR systems. *Magn Reson Med.* 2006; 56:481-488.

77. Konings MK, Bartels LW, Smits HF, Bakker CJ. Heating around intravascular guidewires by resonating RF waves. *J Magn Reson Imaging.* 2000;12: 79-85.

78. Rube MA, Holbrook AB, Cox BF, Houston JG, Melzer A. Wireless MR tracking of interventional devices using phase-field dithering and projection reconstruction. *Magn Reson Imaging.* 2014;32: 693-701.

79. Krieger A, Song S-E, Cho NB, Iordachita II, Guion P, Fichtinger G, et al. Development and evaluation of an actuated MRI-compatible robotic

system for MRI-guided prostate intervention. *IEEE ASME Trans Mechatron*. 2013;18:273-284.

80. El Bannan K, Chronik BA, Salisbury SP. Development of an MRI-compatible, compact, rotary-linear piezoworm actuator. *J Med Device*. 2015;9:014501.

81. Wang Y, Cole GA, Su H, Pilitsis JG, Fischer GS. MRI compatibility evaluation of a piezoelectric actuator system for a neural interventional robot. Paper presented at: Engineering in Medicine and Biology Society, 2009. EMBC 2009. Annual International Conference of the IEEE, 2009.

82. Sutherland GR, Latour I, Greer AD, Fielding T, Feil G, Newhook P. An Image-guide magnetic resonance-compatible surgical robot. *Neurosurgery*. 2008;62:286-293.

83. Sutherland GR, Latour I, Greer AD. Integrating an image-guided robot with intraoperative MRI. *IEEE Eng Med Biol*. 2008;27:59-65.

84. Stoianovici D, Patriciu A, Petrisor D, Mazilu D, Kavoussi L. A new type of motor: pneumatic step motor. *IEEE ASME Trans Mechatron*. 2007;12:98-106.

85. Stoianovici D, Kim C, Petrisor D, Jun C, Lim S, Ball MW, et al. MR safe robot, FDA clearance, safety and feasibility of prostate biopsy clinical trial. *IEEE ASME Trans Mechatron*. 2017;22:115-126.

86. Su H, Cardona DC, Shang W, Camilo A, Cole GA, Rucker DC, et al. A MRI-guided concentric tube continuum robot with piezoelectric actuation: a feasibility study, Paper presented at: IEEE International Conference on Robotics and Automation (ICRA). May 14-18, 2012; Minnesota, USA.

87. Sajima H, Kamiuchi H, Kuwana K, Dohi T, Masamune K. MR-safe pneumatic rotation stepping actuator. *J Robot Mechatron*. 2012;24:820-826.

88. Chen Y, Mershon CD, Tsz Z, Tse HA. 10-mm MR-conditional unidirectional pneumatic stepper motor. *IEEE ASME Trans Mechatron*. 2015;20:782-788.

89. Chen Y, Kwok KW, Tse ZTH. An MR-conditional high-torque pneumatic stepper motor for MRI-guided and robot-assisted intervention. *Ann Biomed Eng*. 2014;42:1823-1833.

90. Guo Z, Lun T, Chen Y, Su H, Chan D, Kwok K. Novel design of an MR-safe pneumatic stepper motor for MRI-guided robotic interventions, Paper presented at: Proceedings of The Hamlyn Symposium on Medical Robotics. June 25-28, 2016; London, UK.

91. Su H, Cole GA, Fischer GS. High-field MRI-compatible needle placement robots for prostate interventions: pneumatic and piezoelectric approaches. *Adv Robot Virtual Reality*. 2012:3-32.

92. Whitney JP, Chen T, Mars J, Hodgins JK. A hybrid hydrostatic transmission and human-safe haptic telepresence robot, Paper presented at: IEEE International Conference on Robotics and Automation (ICRA). May 16-21, 2016; Stockholm, Sweden.

93. Burkhard N, Frishman S, Gruebele A, Whitney JP, Goldman R, Daniel B, et al. A rolling-diaphragm hydrostatic transmission for remote MR-guided needle insertion, Paper presented at: IEEE International Conference on Robotics and Automation (ICRA). May 29-June 3, 2017; Singapore.